Research Square

Preprints are preliminary reports that have not undergone peer review.
They should not be considered conclusive, used to inform clinical practice,
or referenced by the media as validated information.

Time-Varying Coronary Artery Deformation: A Dynamic Skinning Framework for Coronary Intervention Planning and Training

Shuo Wang
Tsinghua University
Tong Ren
The Six medical center of PLA General Hospital
Nan Cheng
The Six medical center of PLA General Hospital
Rong Wang
The Six medical center of PLA General Hospital
Li Zhang
zli@mail.tsinghua.edu.cn

Tsinghua University

Research Article

Keywords: Coronary Artery, Dynamic Modeling, Skeletal Skinning, Intervention Simulation, Open Source

Posted Date: May 30th, 2025

DOI: https://doi.org/10.21203/rs.3.rs-6520074/v1

License: This work is licensed under a Creative Commons Attribution 4.0 International License.
Read Full License

Additional Declarations: No competing interests reported.

Time-Varying Coronary Artery Deformation: A Dynamic Skinning Framework for Coronary Intervention Planning and Training

Shuo Wang[1], Tong Ren[2], Nan Cheng[2], Rong Wang[2], Li Zhang[1*]

[1] Department of Engineering Physics, Key Laboratory of Particle and Radiation Imaging, Ministry of Education, Tsinghua University, Beijing, China

[2] Department of Adult Cardiac Surgery, Senior Department of Cardiology, The Six medical center of PLA General Hospital, Beijing, China

*** Correspondence:**

Li Zhang

zli@mail.tsinghua.edu.cn

Abstract

Background Coronary artery disease remains a leading cause of mortality worldwide, with interventional procedures requiring precise understanding of vessel dynamics. Existing modeling approaches struggle to balance anatomical accuracy with real-time performance when representing coronary deformation throughout the cardiac cycle. This limitation hinders the development of effective surgical simulation platforms for training and preoperative planning, creating a need for dynamic modeling frameworks that can accurately capture time-varying vessel morphology while supporting interactive manipulation.

Methods We developed a computational framework based on biharmonic energy minimization for skinning weight calculation, incorporating volumetric discretization through tetrahedral mesh

generation. The method implements temporal sampling and interpolation for continuous vessel deformation throughout the cardiac cycle, with mechanical constraints and volume conservation enforcement. The framework was validated using clinical datasets from 5 patients, comparing interpolated deformation results against ground truth data obtained from frame-by-frame segmentation across cardiac phases.

Results The proposed framework effectively handled interactive vessel manipulation. Geometric accuracy evaluation showed mean Hausdorff distance of 4.96 ± 1.78 mm and mean surface distance of 1.78 ± 0.75 mm between interpolated meshes and ground truth models. The Branch Completeness Ratio achieved 1.82 ± 0.46, while Branch Continuity Score maintained 0.84 ± 0.06 (scale 0-1) across all datasets. The system demonstrated capability in supporting real-time guidewire-vessel collision detection and contrast medium flow simulation throughout the complete coronary tree structure.

Conclusion Our skinning weight-based methodology enhances model interactivity and applicability while maintaining geometric accuracy. The framework provides a more flexible technical foundation for virtual surgical training systems, demonstrating promising potential for both clinical practice and medical education applications. The code is available at https://github.com/ipoirot/DynamicArtery.

Keywords Coronary Artery, Dynamic Modeling, Skeletal Skinning, Intervention Simulation, Open Source

1 Background

Cardiovascular diseases, particularly coronary artery disease, remain one of the leading causes of mortality worldwide [1]. Accurate representation of coronary artery dynamics has become increasingly critical for evidence-based clinical decision making, spanning from diagnostic assessment to interventional planning [2,3]. The integration of dynamic coronary modeling into clinical workflows

represents a significant opportunity to enhance medical information systems and support patient-specific treatment decisions.

The application of computational modeling in coronary artery analysis has demonstrated remarkable capabilities in providing temporal and spatial distributions of hemodynamic parameters. These analyses enable clinicians to make more informed decisions by quantifying wall shear stress patterns and understanding atherosclerotic plaque progression mechanisms [4,5]. Recent studies have shown that incorporating dynamic vessel behavior into clinical information systems can significantly improve risk stratification and intervention planning compared to static imaging approaches [6,7].

In the context of medical education and interventional training, dynamic modeling has proven effective in enhancing procedural competency and reducing complications [9,10,11]. The ability to visualize and interact with realistic vessel deformation has become particularly important for optimizing stent placement strategies and predicting post-intervention outcomes [12], directly impacting clinical decision making.

However, the implementation of accurate dynamic coronary modeling in medical information systems faces substantial challenges. The complex anatomical characteristics of coronary arteries, including their cyclic motion patterns, multiple branches, and variable geometry, demand sophisticated computational approaches that can capture these nuanced behaviors while maintaining clinical usability. Current clinical information systems typically rely on simplified vessel representations that fail to incorporate the full spectrum of dynamic behavior needed for comprehensive decision support.

Technical challenges in integrating dynamic coronary models into clinical workflows include balancing computational efficiency with anatomical accuracy, ensuring compatibility with existing medical information systems, and providing intuitive visualization tools for clinical interpretation. While recent advances in mesh morphing techniques show promise [13], there remains a critical need

for integrated approaches that can support the entire spectrum of clinical applications from diagnosis to intervention planning.

To address these challenges in transforming medical imaging data into clinically useful decision support tools, we propose a novel framework that combines advanced image processing with skeletal skinning approaches. Our key innovations include:

(1) A robust dynamic tracking method that maintains natural vessel deformation through intelligent interpolation, enhancing the reliability of derived clinical parameters.

(2) Generation of topologically consistent meshes across all cardiac phases, significantly improving the accuracy of hemodynamic assessments for clinical decision making.

(3) Interactive visualization capabilities that enable clinicians to explore vessel dynamics and simulate interventional scenarios in real-time.

This integrated approach bridges the gap between advanced computational modeling and practical clinical applications, providing a robust foundation for enhancing medical information systems and supporting evidence-based interventional planning.

2 Methods and materials

Our methodology for generating dynamic coronary artery models follows a comprehensive workflow as illustrated in Fig. 1. Beginning with 4D-CCTA data acquisition (yellow frame), we extract end-diastolic coronary images as the foundation for subsequent processing. The workflow proceeds through three key technical stages: coronary arterial tree construction (purple frame, Section 2.2), which involves vessel segmentation, centerline extraction, branch identification, and surface mesh generation; coronary artery skinning weight calculation (green frame, Section 2.3), which applies specialized skinning techniques and weight parameters to control vessel deformation; and dynamic sequence

generation (blue frame, Section 2.4), which produces the final motion simulation with distinct color-coding for left (red) and right (blue) coronary artery branches. This integrated approach combines anatomical precision with realistic motion characteristics to create clinically valuable simulations for assessment and treatment planning.

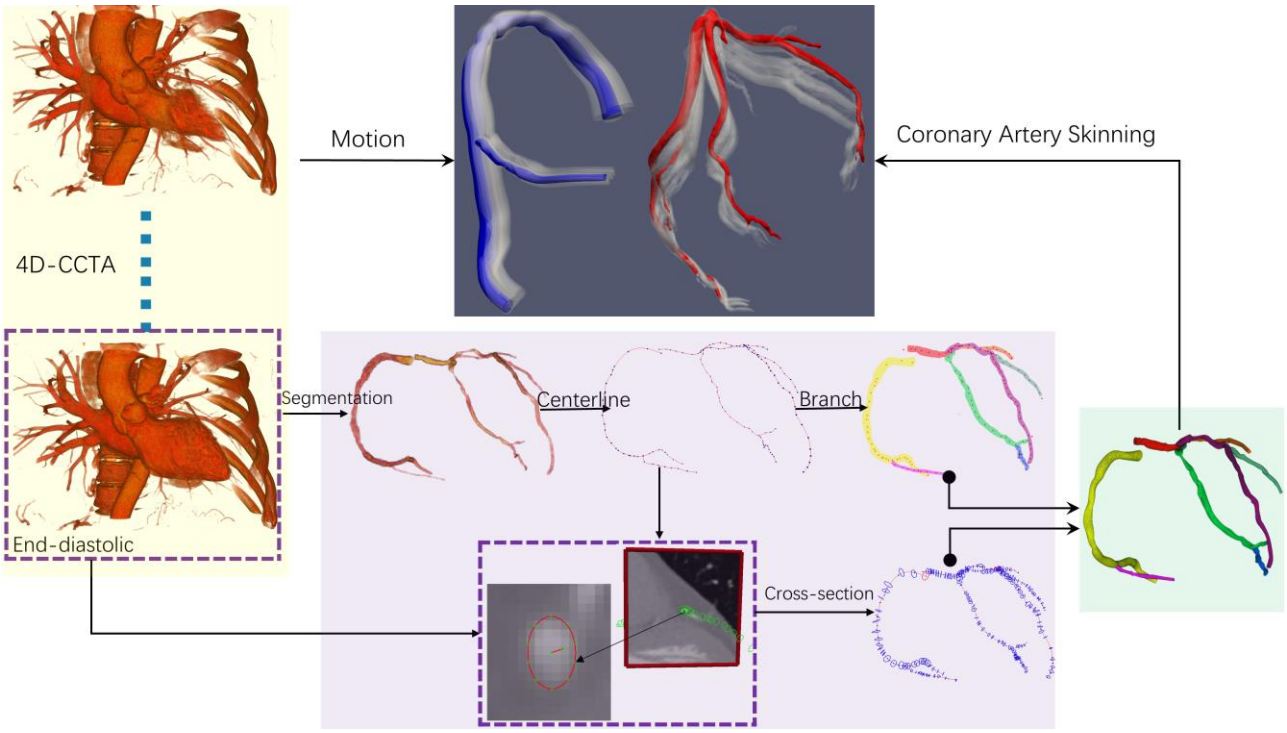


Fig. 1 Comprehensive workflow for dynamic coronary artery model generation.

2.1 CT data collection

Cardiac CT imaging was performed using a Revolution Apex scanner (GE Healthcare, Milwaukee, WI, USA) during end-expiratory breath-hold with the patient in normal sinus rhythm. Image reconstruction was conducted across 20 temporal phases of the cardiac cycle, spanning from -5% to 106% of the R-R interval. The acquisition parameters included an isotropic slice thickness and increment of 0.625 mm, with an in-plane spatial resolution of 0.23 × 0.23 mm. The mean effective radiation dose, calculated in accordance with European Guidelines for Quality Criteria for Computed Tomography, was 10.49 mSv.

2.2 Construction of Coronary Arterial Tree Model

The construction of an anatomically accurate coronary arterial tree model involves multiple sophisticated steps, beginning with medical image acquisition and proceeding through several processing stages. The process integrates both imaging data and anatomical knowledge to ensure physiological accuracy.

2.2.1 Vessel Segmentation and Centerline Extraction

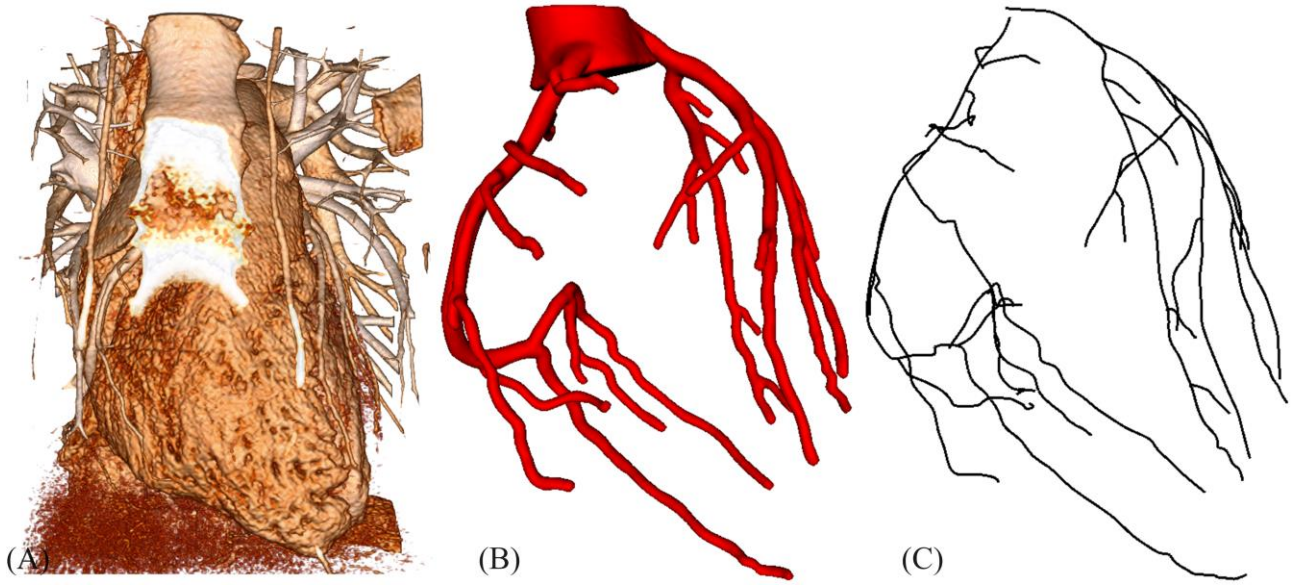


Fig. 2 Coronary artery segmentation workflow. (A) Volume rendering of cardiac CTA data. (B) Segmented coronary artery mask using Frangi vesselness filter. (C) Extracted vessel centerlines using fast marching algorithm.

The coronary artery segmentation is performed on end-diastolic CTA images (Fig.2(A)), where vessels are maximally dilated with optimal contrast enhancement and minimal motion artifacts. The process employs the Frangi vesselness filter [14], which is based on the analysis of the Hessian matrix eigenvalues to detect tubular structures. For a given scale σ, the vesselness measure $V_0(s)$ is defined as, where s represents the spatial position in the image volume:

$$V_0(s) = \begin{cases} 0 & \text{, if } \lambda_2 > 0 \text{ or } \lambda_3 > 0 \\ \left(1 - e^{-\frac{{R_A}^2}{2\alpha^2}}\right) e^{-\frac{{R_B}^2}{2\beta^2}} \left(1 - e^{-\frac{S^2}{2c^2}}\right) & \text{,otherwise} \end{cases}$$

where $R_A = \left|\frac{\lambda_2}{\lambda_3}\right|$ is ratio for distinguishing between plate and line structures, $R_B = \frac{|\lambda_1|}{\sqrt{\lambda_2 \lambda_3}}$ is ratio for distinguishing blob-like structures; λ_1, λ_2, and λ_3 are eigenvalues of the Hessian matrix; $S = \sqrt{{\lambda_1}^2 + {\lambda_2}^2 + {\lambda_3}^2}$ is Frobenius norm of the Hessian, α, β, and c are thresholds controlling the sensitivity of the filter. The final vesselness measure V (Fig.2(B)) is obtained by computing the maximum response over a range of scales:

$$V = max_{\sigma_{min} < \sigma < \sigma_{max}} V_0(s)$$

where σ represents the scale parameter (in mm), σ_{min} and σ_{max} define the range of vessel sizes to be detected (typically $\sigma_{min} = 0.5$ mm and $\sigma_{max} = 2.5$ mm for coronary arteries).

Following segmentation, centerline extraction is performed using a fast marching algorithm [8] combined with backtracking (Fig.2(C)). The centerline coordinates are represented as a series of points $P_i(x_i, y_i, z_i)$, where each point carries additional information about vessel radius r, and bifurcation relationships.

2.2.2 Topology Analysis and Branch Identification

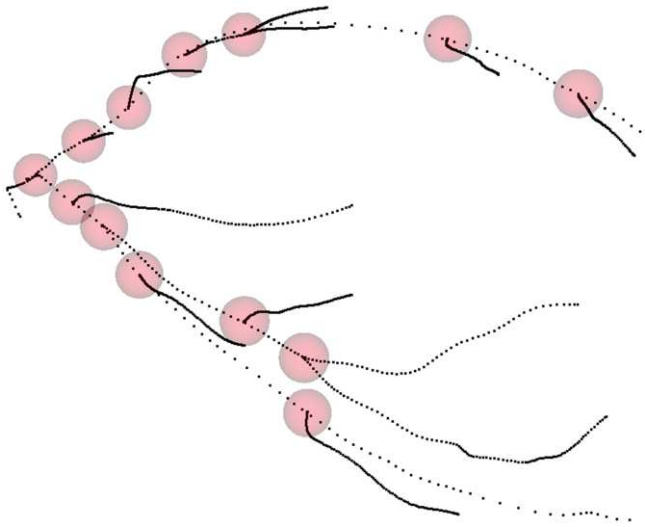


Fig. 3 Branch point detection in left coronary artery. Red spheres indicate the detected bifurcation points along the vessel centerlines.

The arterial tree topology is analyzed using a hierarchical approach. Starting from the main coronary arteries (left main, left anterior descending, left circumflex, and right coronary artery), branches are identified and classified based on their anatomical positions and geometric features. As shown in Fig. 3, branch points are characterized by their bifurcation angles and cross-sectional area ratios, following Murray's law for physiological branching patterns [15]:

$$r_p^3 = r_{d1}^3 + r_{d2}^3$$

where r_p is the parent vessel radius, r_{d1} and r_{d2} are daughter vessel radii.

2.2.3 Surface Mesh Generation

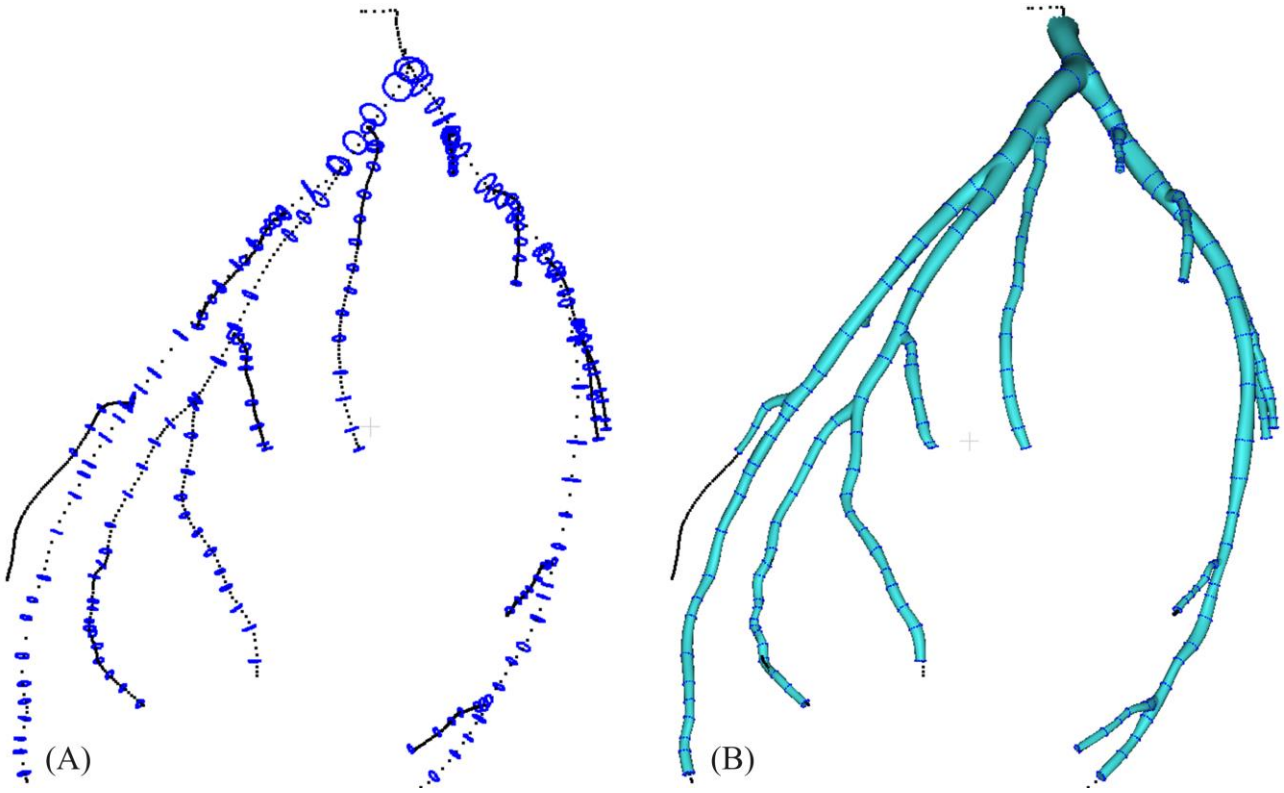


Fig. 4 Surface reconstruction of coronary arteries. (A) Cross-sections with arbitrary shaped contours extracted along the centerline using Frenet-Serret trihedron. (B) Final smooth surface representation generated by B-spline interpolation between cross-sectional patches.

The vessel surface is reconstructed using a hybrid approach combining implicit surface fitting and explicit mesh generation. Cross-sections are positioned along the parameterized centerline using the Frenet-Serret trihedron (Fig. 4(A)). For each cross-section, the patch pattern is generated using a central point and an arbitrary shaped outer contour in the trihedron normal-binormal plane, following the approach of Vukicevic et al. [16]. These cross-sectional patches are then connected using B-spline interpolation to create a smooth surface representation (Fig. 4(B)). The surface mesh is generated using an advancing front method, with mesh density adapted according to local geometric features:

$$h(x) = h_{min} + (h_{max} - h_{min})e^{-\alpha\kappa(x)}$$

where h(x) is the local mesh size, κ(x) is the local curvature, and α is a control parameter.

2.3 Coronary Artery Skinning Weight Calculation

The computation of skinning weights for coronary artery deformation follows a comprehensive anatomical framework that ensures both robustness and physiological fidelity. The process begins with a preprocessing stage that handles the input coronary artery mesh $M = (V, F)$, where a cleaning operation is performed to ensure topological consistency and remove artifacts from medical imaging reconstruction. This operation produces a cleaned vessel mesh M_{clean} that serves as the foundation for subsequent computations.

An important step in our approach is the volumetric discretization of the arterial wall through tetrahedral mesh generation. We employ constrained Delaunay tetrahedralization to create a volumetric representation $T = (V_T, T_T)$ that encompasses both the vessel wall geometry and the centerline structure, where V_T represents the set of vertices in the volumetric mesh, T_T represents the set of tetrahedral elements, each defined by four vertex indices. This process carefully preserves the anatomical characteristics of coronary arteries while ensuring that each tetrahedron maintains a minimum volume threshold of 10^{-7}mm^3 to prevent numerical instabilities in subsequent computations.

The weight computation follows a biharmonic energy minimization framework, where we solve for weights W that minimize the biharmonic energy while satisfying vessel wall constraints. The optimization problem is formulated as:

$$\min_{w_b} \int_{\Omega} \|\Delta w_b(v)\|^2 dv$$

subject to boundary conditions that enforce unity weights at centerline locations and zero weights at vessel wall boundaries, where w_b represents the skinning weight function for the b-th centerline segment, Δ is the Laplacian operator measuring second spatial derivatives, v denotes a point in 3D space within the vessel wall domain Ω, and dv is the differential volume element. This continuous optimization is discretized and solved using an active set method with careful constraint handling to maintain both boundedness ($0 \leq w_{b(v)} \leq 1$) and partition of unity ($\sum_b w_{b(v)} = 1$).

The numerical solution employs an efficient sparse matrix formulation, where the discrete bi-Laplacian operator L is constructed to capture the geometric properties of the arterial wall mesh. The boundary conditions are encoded through constraint matrices, leading to the discrete optimization problem:

$$\min_W tr(W^T L\, W) \quad subject\ to: BW = D$$

where W is the weight matrix (columns for centerline segments, rows for mesh vertices), L is the discrete bi-Laplacian operator matrix, $tr(\cdot)$ denotes the matrix trace operator, and the constraint $BW = D$ encodes boundary conditions, with B being the constraint matrix and D containing the boundary values. This discrete formulation corresponds to the continuous energy minimization problem, where $tr(W^T L\, W)$ represents the discretized version of $\int_\Omega \|\Delta w_b(v)\|^2 dv$ in the continuous domain.

To ensure numerical stability and physiological validity, the computed weights undergo a normalization process that enforces the partition of unity constraint while preserving the relative influence of each centerline segment. This is achieved through row-wise normalization:

$$w_{i,j} = \frac{w_{i,j}}{\sum_k w_{i,k}}$$

where i for vertex index on the vessel wall mesh, j for centerline segment index, and k as the summation variable iterating through all centerline segments.

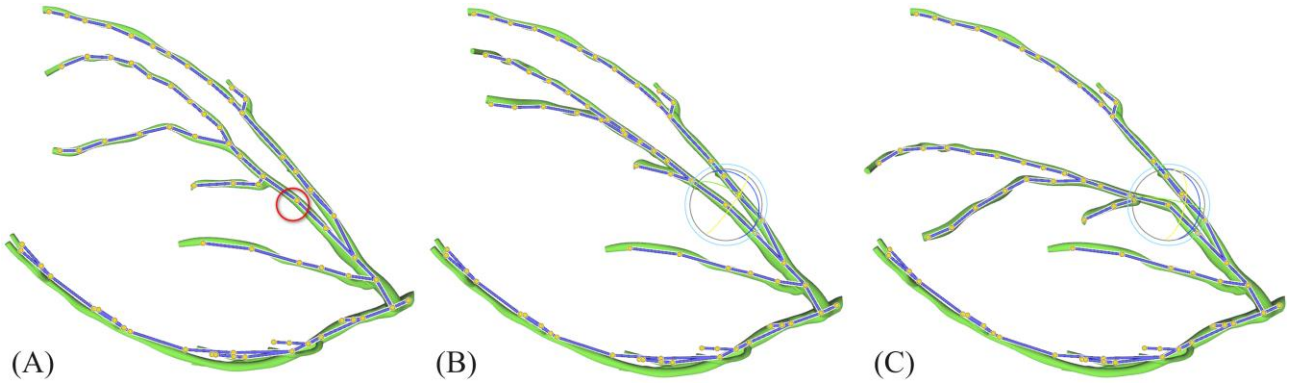


Fig. 5 Coronary artery deformation using skinning weight calculation. (A) Original left coronary artery mesh with deformation skeletal nodes marked in red circles. (B) Result after first deformation. (C) Result after second deformation.

The weight distribution method ensures smooth variation across vessel walls while maintaining local control and non-negative weights, crucial for preserving vessel wall continuity during cardiac motion-induced deformation. This mathematically rigorous and physiologically accurate approach effectively handles complex arterial structures through efficient sparse matrix operations, outperforming traditional weight computation methods in capturing the intricate relationships between centerline segments and vessel wall geometry. The coronary artery deformation process is demonstrated in Fig. 5. Starting with the original mesh and deformation skeletal nodes (Fig. 5(A)), the artery underwent two successive deformations (Fig. 5(B) and Fig. 5(C)) using our skinning weight calculation method. The complete deformation validation process can be visualized as shown in the animation (Additional file 3).

2.4 Dynamic Sequence Generation for Coronary Artery Motion

Dynamic sequence generation for coronary artery motion is a comprehensive process that creates realistic vessel deformation patterns throughout the cardiac cycle. The process begins with temporal sampling and interpolation, where the cardiac cycle is divided into 20 temporal phases, spanning from -5% to 106% of the R-R interval. Key poses at these phases serve as anchors, while intermediate frames between captured phases are generated through temporal interpolation using the formula:

$$P(t) = (1 - t)\, P_1 + t\, P_2$$

where P_1 and P_2 represent consecutive key poses, and t varies between 0 and 1.

The centerline evolution forms the backbone of the motion sequence, described by a time-dependent curve

$$C(s,t) = \big(x(s,t), y(s,t), z(s,t)\big)$$

where s represents the arc-length parameter and t denotes time. The tangent vector $T(s,t) = \frac{\partial C}{\partial s}$ represents the local vessel direction, while the curvature $\kappa(s,t) = \left\|\frac{\partial^2 C}{\partial s^2}\right\|$ characterizes the bending of the vessel. These quantities are constrained to satisfy $|\kappa(s,t)| \leq \kappa_{max}$ to prevent unrealistic sharp bends during the cardiac cycle. The vessel cross-section undergoes simultaneous deformation, modeled as an ellipse with time-varying parameters following the equation:

$$\frac{x^2}{a(t)^2} + \frac{y^2}{b(t)^2} = 1$$

where $a(t)$ and $b(t)$ represent the major and minor axis lengths. The cross-sectional area follows the volume conservation law:

$$\pi a(t) b(t) = A_0\big(1 + \epsilon_r(t)\big)$$

where A_0 is the reference cross-sectional area and $\epsilon_r(t)$ represents the small radial strain that accounts for the vessel's slight compressibility during the cardiac cycle, typically within ±5% range.

The motion sequence must adhere to various anatomical and mechanical constraints. These include maximum bending angles θ_{max}, minimum radius of curvature R_{min}, and strain limits ϵ_{max} to ensure physiologically plausible coronary artery movements during the cardiac cycle.

The velocity field, computed as $v(x,t) = \frac{\partial P}{\partial t}$, undergoes regularization through the equation:

$$\nabla^2 v + \lambda \frac{\partial v}{\partial t} = 0$$

where λ serves as a smoothing parameter to ensure fluid-like motion transitions.

To maintain realistic motion sequences, we enforce temporal coherence through position constraints between consecutive frames: $\|P(t+\Delta t) - P(t)\| \leq \delta$, where δ is the maximum allowed displacement threshold between adjacent frames to ensure smooth motion transitions. Additionally, periodic boundary conditions ensure that $P(T) = P(0)$, where T represents the cardiac cycle period. The quality of the generated sequence is evaluated through temporal consistency $E_{temp} = \sum_{t=1}^{N} \|P_t - P_{t-1}\|^2$ and spatial smoothness:

$$E_{spatial}(t) = \sum_{i=1}^{M} \left\|\Delta P_{t,i}\right\|^2$$

where $\Delta P_{t,i} = \sum_{j \in N(i)} (P_{t,j} - P_{t,i})$ represents the discrete Laplacian operator with $N(i)$ denoting the neighborhood of point i. The total spatial energy is then computed as $E_{spatial} = \sum_{t=1}^{N} E_{spatial}(t)$. These terms are combined in a total energy minimization framework $E_{total} = \omega_1 E_{temp} + \omega_2 E_{spatial}$.

This comprehensive approach results in a continuous, physically plausible representation of coronary artery motion throughout the cardiac cycle, as shown in Fig. 6. The generated sequences effectively balance mathematical precision with physiological realism while maintaining computational efficiency. The resulting dynamic sequences provide valuable insights into vessel behavior and serve as essential tools for both visualization and biomechanical analysis in clinical applications. The accuracy of these sequences directly impacts the quality of subsequent analyses and simulations, making the generation process a critical component in understanding coronary artery dynamics.

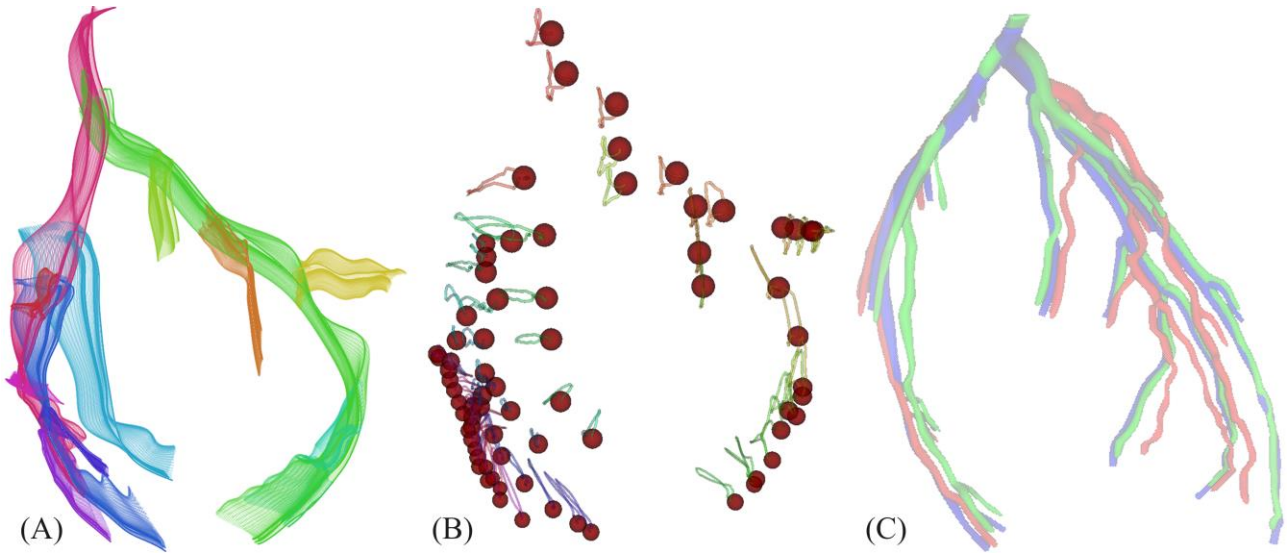


Fig. 6 Visualization of coronary artery dynamic sequence generation. (A) Temporal evolution of left coronary artery centerlines, where different colors denote distinct arterial branches with preserved geometric continuity. (B) Trajectory analysis depicting initial anatomical positions (red spheres) and their corresponding motion paths (semi-transparent tubes) under prescribed displacement constraints. (C) Multi-phase visualization of left coronary artery meshes at three temporal positions within the cardiac cycle, demonstrating the dynamic deformation of vessel cross-sections.

3 Results

3.1 Validation of Dynamic Mesh Generation

To rigorously validate the accuracy of our proposed dynamic mesh generation framework, we conducted comprehensive experiments on five independent 4D CT datasets. We present a detailed analysis of one representative case comprising 20 temporal phases, while similar validation procedures were performed across all five datasets. The validation strategy employed a systematic approach where meshes at even-numbered phases (0, 2, 4, ...) were reconstructed using direct tracking-based skinning weights, while odd-numbered phases (1, 3, 5, ...) were generated through our interpolation method utilizing adjacent frame information. Notably, while traditional segmentation-based methods often suffer from incomplete branch reconstruction due to motion artifacts across different cardiac phases, our skinning weights-based approach demonstrates significant advantages in maintaining coronary tree completeness. By using end-diastolic phase as the reference, where coronary arteries are most clearly visible and complete, our method successfully preserves the integrity of the branching structure throughout the cardiac cycle. This approach effectively addresses a common limitation in conventional segmentation methods, where motion artifacts frequently result in discontinuous or missing branches in various phases.

For quantitative assessment, we established a ground truth dataset by performing frame-by-frame segmentation and reconstruction across all 20 phases, represented as green meshes $M^*(t)$. The interpolated meshes at odd-numbered phases, denoted as $M_I(t)$, were rendered in red for visual comparison. This experimental design enables direct evaluation of our interpolation method's accuracy at intermediate phases where direct tracking data is unavailable.

The geometric accuracy of the interpolated meshes was evaluated using the Hausdorff distance (HD) metric:

$$d_H(M_I, M^*) = \max\left(\sup_{x \in M_I} \inf_{y \in M^*} d(x,y), \sup_{y \in M^*} \inf_{x \in M_I} d(x,y)\right)$$

where d_H represents the Hausdorff distance, M_I denotes the interpolated mesh, M^* represents the ground truth mesh, $d(x,y)$ is the Euclidean distance between points x and y, sup denotes the supremum (least upper bound), and inf denotes the infimum (greatest lower bound). Additionally, we computed the mean surface distance (MSD) to assess overall mesh similarity:

$$MSD(M_I, M^*) = \frac{1}{|M_I|} \sum_{x \in M_I} min_{y \in M^*} d(x,y)$$

where $|M_I|$ represents the total number of vertices in the interpolated mesh, and min denotes the minimum distance from a point x on M_I to any point y on M^*.

To specifically evaluate the topological completeness of coronary trees, we introduced two complementary metrics: Branch Completeness Ratio (BCR) and Branch Continuity Score (BCS). The BCR quantifies the preservation of branch numbers while BCS assesses the structural continuity:

$$BCR = \frac{N_I}{N_R}, \quad BCS = \frac{1}{N_I} \sum_{i=1}^{N_I} \left(\frac{L_i}{L_R^i}\right)$$

where N_I and N_R represent the number of detected branches in the interpolated and reference meshes respectively, L_i denotes the length of the i-th branch in the interpolated mesh, and L_R^i is its corresponding length in the reference mesh. Together, these metrics provide a comprehensive assessment of both topological preservation and structural continuity of the coronary tree during the interpolation process.

Phase	HD (mm)	MSD(mm)	BCR	BCS
01	5.75	1.49	2.5	0.83
03	7.7	3.39	1.66	0.76
05	6.79	2.75	5.0	0.71
07	8.2	2.97	2.5	0.75
09	2.27	0.93	1.25	0.89
11	5.88	2.36	1.0	0.85
13	5.0	2.55	1.66	0.82
15	0.79	0.11	1.0	0.95
17	3.47	0.97	1.66	0.87
19	8.34	2.39	1.25	0.77
Mean	5.42	1.99	1.95	0.82
STD	2.6	1.03	1.18	0.07



Fig. 7 Quantitative evaluation metrics for coronary artery mesh interpolation showing individual phase analysis for Dataset #1 (representative case), demonstrating the interpolation accuracy across different phases of the cardiac cycle.

The quantitative evaluation results are summarized in Fig.7 and Fig.8. Fig.7 presents a detailed phase-by-phase analysis for the representative case (Dataset #1) corresponding to the visual results shown in Fig. 9. This comprehensive temporal analysis demonstrates the consistency of our interpolation method across different cardiac phases.

Dataset	HD (mm)	MSD (mm)	BCR	BCS
#1	6.23	2.16	2.0	0.81
#2	3.89	1.28	1.5	0.88
#3	7.16	2.89	2.5	0.75
#4	4.57	1.56	1.8	0.84
#5	2.95	0.99	1.3	0.9
Mean	4.96	1.78	1.82	0.84



Fig. 8 Quantitative evaluation metrics for coronary artery mesh interpolation across five 4D CT datasets, presenting summary statistics that demonstrate the overall performance and consistency of our method across multiple clinical cases.

Examining the detailed results from Fig.7 for the representative case, our interpolation method demonstrates robust performance across different cardiac phases. For Dataset #1, the HD exhibits a mean of 5.42 ± 2.60 mm, while the MSD shows better consistency with 1.99 ± 1.03 mm, indicating generally reliable geometric accuracy of the interpolated meshes. The BCR (1.95 ± 1.18) consistently exceeds 1.0, suggesting that our method effectively preserves and sometimes enhances branch detection compared to the reference meshes, addressing the common challenge of incomplete branch reconstruction in traditional segmentation-based approaches. The BCS maintains a high average of 0.82 ± 0.07, with values ranging from 0.71 to 0.95, demonstrating stable structural continuity preservation throughout the cardiac cycle. Notably, phases with lower geometric distances (e.g., Phase 15 with HD = 0.79 mm, MSD = 0.11 mm) achieve higher continuity scores (BCS = 0.95), confirming the correlation between geometric accuracy and topological preservation.

Fig.8 summarizes the performance across all five datasets, where each dataset value represents the mean across all interpolated phases. The evaluation metrics include geometric accuracy measures (HD and MSD) and topological preservation measures (BCR and BCS). These results quantitatively validate that our proposed method achieves both accurate geometric interpolation and robust topological preservation of the coronary tree structure throughout the cardiac cycle.

The complete processing pipeline for a 4D CT dataset is demonstrated in the animation (Additional file 1), showing the key steps of segmentation, temporal interpolation, and visualization of the dynamic coronary tree model.

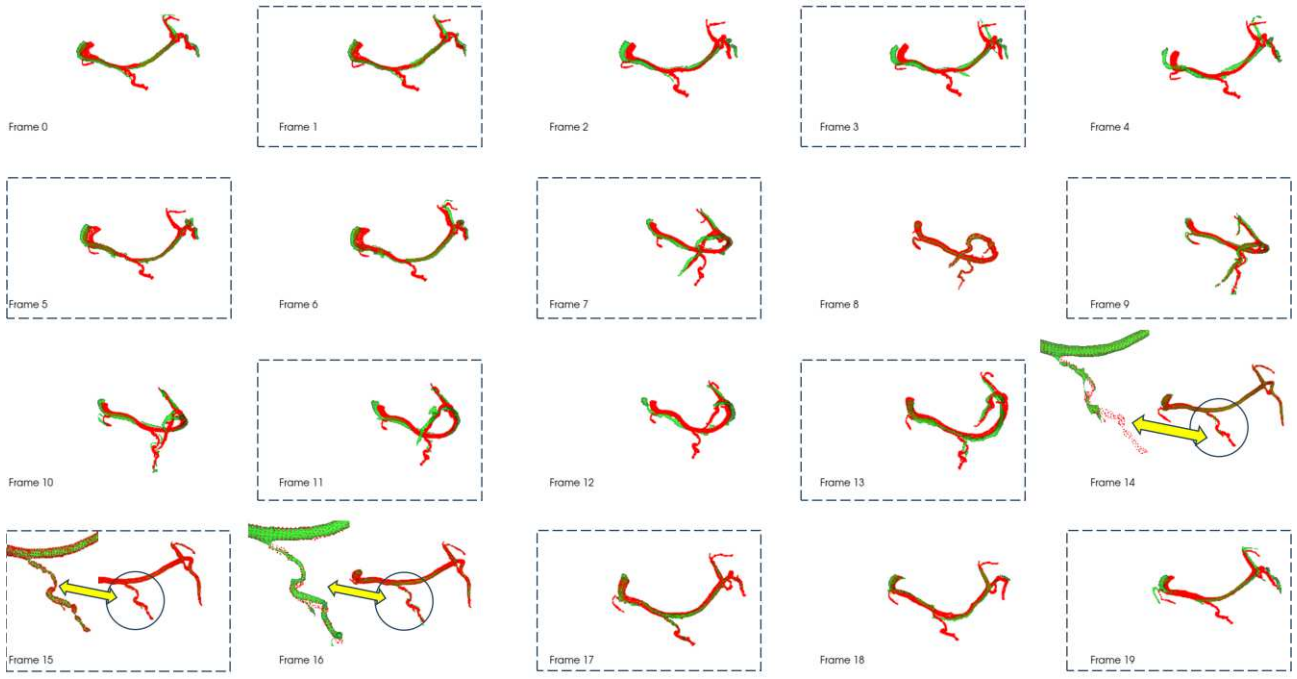


Fig. 9 Visual comparison of coronary artery meshes over a cardiac cycle. Twenty phases (0-19) arranged in 4×5 grid show interpolated meshes (red) overlaid with ground truth segmentations (green). Dashed-border frames (1,3,5,7...) represent interpolated phases, while others (0,2,4,6,...) were reconstructed using direct tracking-based weights. Consistent mesh overlap demonstrates anatomical accuracy throughout the cycle. Magnified views of frames 14-16 show successful mesh reconstruction in frame 15 despite tracking loss in frame 14.

3.2 Validation Through Application: PCI Simulation

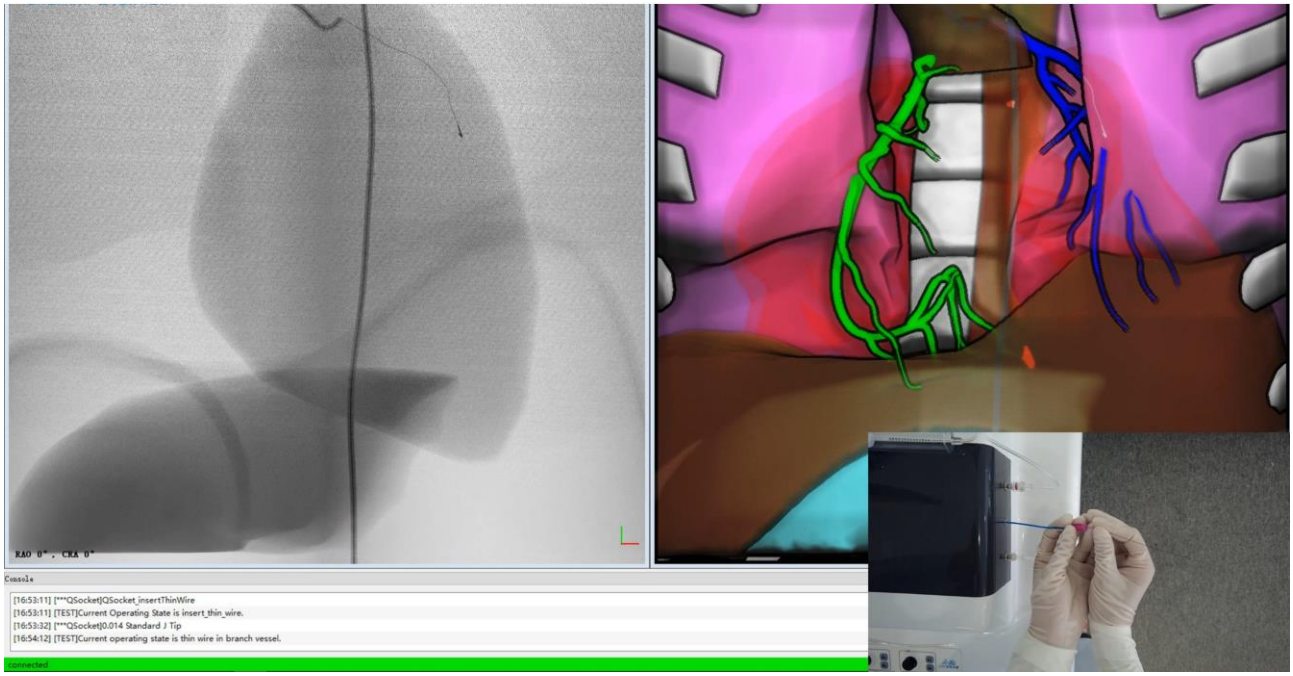


Fig. 10 Real-time coronary intervention simulation. Left: Simulated X-ray fluoroscopic view showing the results of real-time collision detection and physical simulation of guidewire-vessel interaction. Right: Corresponding 4D anatomical scene with dynamic vessel deformation. Bottom right: PCI simulator hardware configuration.

To demonstrate the practical utility of our dynamic mesh reconstruction framework, we integrated it into a coronary intervention simulation system (Fig. 10). This integration enables realistic catheterization training scenarios with accurate vessel deformation and fluid dynamics simulation throughout the cardiac cycle. The simulation framework incorporates two critical components: (1) real-time collision detection between the guide wire and dynamically deforming coronary arteries, as shown in Fig. 10, and (2) contrast medium flow simulation within the complete coronary tree structure (Fig. 11).

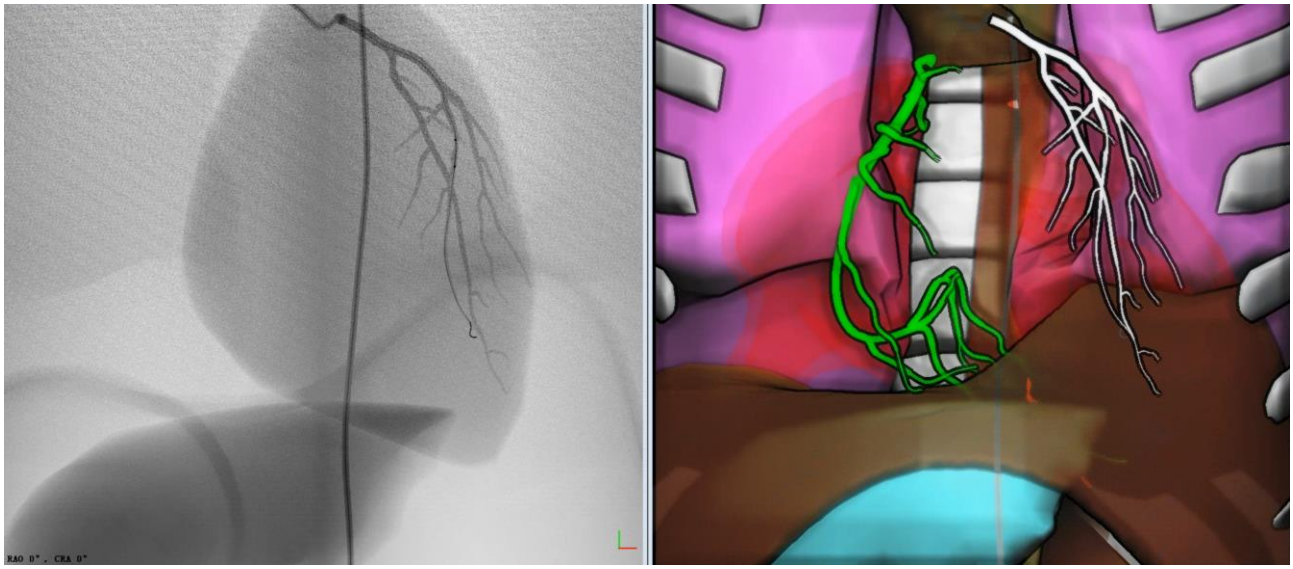


Fig. 11 Simulated LCA contrast injection. The fluoroscopic sequence demonstrates dynamic contrast medium opacification throughout the left coronary tree during the cardiac cycle.

Our dynamic mesh generation method provides essential support for both aspects: For guide wire navigation simulation, we implemented a dense collision detection algorithm between the discrete guide wire elements and the temporally varying coronary mesh. The complete topological structure maintained by our method ensures continuous collision response as the guide wire navigates through different branches. The collision detection is performed using a hierarchical bounding volume structure that is updated according to the mesh deformation at each cardiac phase, enabling efficient real-time performance while maintaining accuracy. The contrast medium simulation leverages our preserved vessel topology to accurately model fluid dynamics within the coronary tree. We adopted a particle-based fluid simulation approach where the complete and continuous vessel structure is essential for realistic contrast medium propagation. The dynamic mesh sequence provides accurate boundary conditions for the fluid simulation, allowing the contrast medium to flow naturally through the deforming vessels while respecting the cardiac motion.

The simulation results demonstrate that our dynamic mesh generation method effectively supports both the mechanical aspects (guide wire-vessel interaction) and fluid dynamics (contrast medium flow) required for realistic coronary intervention simulation. The preserved topological completeness and geometric accuracy of the vessel structure throughout the cardiac cycle prove crucial for achieving high-fidelity simulation outcomes. Real-time coronary intervention simulation as shown in the animation (Additional file 2).

4 Discussion

Our skeletal skinning weights-based dynamic modeling framework for coronary arteries demonstrates significant advantages over recent image registration-based methods [17]. Our approach, utilizing biharmonic energy minimization for deformation weight computation, enables precise vessel morphology control while extending traditional CFD analysis capabilities.

The framework represents a significant advancement in virtual surgical training applications. The skinning weights-based approach enables clinicians to modify vessel morphology through control points, rapidly adapting to individual patient anatomy. Tetrahedral mesh generation ensures robust weight computation, while the biharmonic energy minimization framework guarantees smooth weight distribution across vessel walls.

Our dynamic mesh generation framework has been successfully integrated into real-time surgical simulation, supporting guidewire-vessel collision detection and contrast medium flow simulation, providing effective tools for pre-operative simulation and surgical planning.

While the current framework shows promising results, certain limitations and future directions warrant consideration. Computational efficiency requires optimization, particularly for real-time deformation of complex branching structures, and further validation is needed for deformation

accuracy across various pathological conditions. While Psiuk-Maksymowicz et al.'s approach excels in CFD analysis, our method's capability for interactive manipulation and real-time deformation makes it particularly suitable for virtual reality-based surgical training and education. This complementary advancement suggests that future developments might benefit from combining both approaches to create more comprehensive solutions for cardiovascular modeling and simulation.

5 Conclusions

This paper presents a novel dynamic modeling framework for coronary arteries based on anatomically-driven skeletal skinning weights. Through the implementation of biharmonic energy minimization and volumetric discretization, we have demonstrated the capability to generate physiologically accurate vessel deformations that maintain anatomical integrity throughout the cardiac cycle. This approach significantly enhances the information content available to clinicians for diagnostic assessment and interventional planning.

Unlike traditional approaches that focus solely on static visualization or computational fluid dynamics, our framework enables clinicians to interactively explore vessel dynamics and simulate interventional scenarios while preserving mechanical constraints and anatomical relationships. This capability directly supports clinical decision making by allowing physicians to evaluate potential intervention strategies and predict their outcomes in a patient-specific context.

Experimental results have validated the framework's effectiveness in maintaining geometric accuracy and topological completeness throughout the cardiac cycle, with mean Hausdorff distances of 4.96 ± 1.78 mm and branch continuity scores of 0.84 ± 0.06 across multiple patient datasets. The integration of our framework into a coronary intervention simulation system demonstrates its practical utility for both clinical education and pre-procedural planning, potentially reducing procedural complications and improving patient outcomes.

The open-source nature of our implementation facilitates further development and integration with existing medical information systems, promoting wider adoption in clinical settings. Future work will focus on enhancing computational efficiency for more complex anatomical configurations and validating the framework's impact on clinical decision making through prospective studies.

This research represents a significant advancement in medical visualization and computational modeling for coronary artery disease, providing clinicians with more comprehensive and interactive tools for evidence-based decision making in both diagnostic and interventional contexts.

Declarations

Ethics approval and consent to participate: This study was conducted in accordance with the declaration of Helsinki. The Ethics Committee of the General Hospital of the Chinese People's Liberation Army accepted this protocol (S2024-580). Informed consent was obtained from all individual participants included in the study.

Consent for publication: Informed consent was obtained from all individual participants included in the study.

Availability of data and materials: The datasets used and/or analysed during the current study available from the corresponding author on reasonable request.

Competing interests: The authors declare that the research was conducted in the absence of any commercial or financial relationships that could be construed as a potential conflict of interest.

Funding: This study was funded by National Natural Science Foundation of China (62031020 and 62476286), National Key R&D Plan(2022YFB4700800), Beijing Science and Technology Plan Project(Z231100005923039).

Author Contributions: Conceptualization, R.W. and T.R.; methodology, S.W. and L.Z.; software, S.W.; validation, T.R., N.C. and R.W.; formal analysis, S.W.; investigation, T.R.; resources, N.C., R.W., S.W. and L.Z.; data curation, T.R. and S.W.; writing—original draft preparation, S.W. and T.R.; writing—review and editing, N.C., R.W. and L.Z.; visualization, S.W.; supervision, N.C., R.W. and L.Z.; funding acquisition, N.C., R.W. and L.Z. All authors have read and agreed to the published version of the manuscript.

Acknowledgements: Not applicable.

6 References

1. Tsao CW, Aday AW, Almarzooq ZI, Anderson CA, Arora P, Avery CL, et al. Heart disease and stroke statistics—2023 update: a report from the American Heart Association. Circulation. 2023;147:e93-621.
2. Taylor CA, Fonte TA, Min JK, Koo BK, Leipsic J, Pontone G. Computational Fluid Dynamics Applied to Cardiac Computed Tomography for Noninvasive Quantification of Fractional Flow Reserve. J Am Coll Cardiol. 2013;61:2233-41. https://doi.org/10.1016/j.jacc.2012.11.083.
3. Morris PD, Ryan D, Morton AC, Lycett R, Lawford PV, Hose DR. Virtual Fractional Flow Reserve From Coronary Angiography: Modeling the Significance of Coronary Lesions. JACC Cardiovasc Interv. 2013;6:149-57. https://doi.org/10.1016/j.jcin.2012.08.024.
4. Chatzizisis YS, Coskun AU, Jonas M, Edelman ER, Feldman CL, Stone PH. Role of Endothelial Shear Stress in the Natural History of Coronary Atherosclerosis and Vascular Remodeling. J Am Coll Cardiol. 2007;49:2379-93. https://doi.org/10.1016/j.jacc.2007.02.059.
5. Stone PH, Maehara A, Coskun AU, Maynard CC, Zaromytidou M, Siasos G, et al. Role of Low Endothelial Shear Stress and Plaque Characteristics in the Prediction of Nonculprit Major Adverse

Cardiac Events. JACC Cardiovasc Imaging. 2018;11:462-71. https://doi.org/10.1016/j.jcmg.2017.01.031.

6. Kwak BR, Bäck M, Bochaton-Piallat ML, Caligiuri G, Daemen MJ, Davies PF, et al. Biomechanical factors in atherosclerosis: mechanisms and clinical implications. Eur Heart J. 2014;35:3013-20. https://doi.org/10.1093/eurheartj/ehu353.
7. Chen Z, Contijoch F, Colvert GM, Manohar A, Kahn AM, Narayan HK, et al. Detection of left ventricular wall motion abnormalities from volume rendering of 4DCT cardiac angiograms using deep learning. Front Cardiovasc Med. 2022;9:919751. https://doi.org/10.3389/fcvm.2022.919751.
8. Jia D, Zhuang X. Directional fast-marching and multi-model strategy to extract coronary artery centerlines. Comput Biol Med. 2019;108:67-77. https://doi.org/10.1016/j.compbiomed.2019.03.029.
9. Ujiie H, Kato T, Igami T, Fujiwara M, Sato M, Nagino M. Developing a Virtual Reality Simulation System for Preoperative Planning of Robotic-Assisted Thoracic Surgery. J Clin Med. 2024;13:611-9. https://doi.org/10.3390/jcm13020611.
10. Joseph FJ, Rai A, Chandra PS, Suri A, Kumar A, Kale SS. Simulation training approaches in intracranial aneurysm surgery-a systematic review. Neurosurg Rev. 2023;46:101-8. https://doi.org/10.1007/s10143-023-01995-5.
11. Gamberini G, Tognarelli S, Saracino A, Menciassi A, Sinibaldi E, Ciuti G. Design and preliminary validation of a high-fidelity vascular simulator for robot-assisted manipulation. Sci Rep. 2024;14:4779-90. https://doi.org/10.1038/s41598-024-55351-8.
12. Han Z, Li J, Singh M, Wu C, Liu C, Zhao X. A review on organ deformation modeling approaches for reliable surgical navigation using augmented reality. Comput Assist Surg. 2024;29:e2357164. https://doi.org/10.1080/24699322.2024.2357164.
13. Pons-Moll G, Romero J, Mahmood N, Black MJ. Dyna: A model of dynamic human shape in motion. ACM Trans Graph. 2015;34:1-14. https://doi.org/10.1145/2766993.

14. Frangi AF, Niessen WJ, Vincken KL, Viergever MA. Multiscale vessel enhancement filtering. Med Image Comput Comput Assist Interv. 1998;1496:130-7. https://doi.org/10.1007/BFb0056195.
15. Murray CD. The physiological principle of minimum work: I. The vascular system and the cost of blood volume. Proc Natl Acad Sci USA. 1926;12:207-14.
16. Vukicevic AM, Stepanovic NM, Jovicic GR, Apostolovic SR, Filipovic ND. Three-dimensional reconstruction and NURBS-based structured meshing of coronary arteries from the conventional X-ray angiography projection images. Sci Rep. 2018;8:1711. https://doi.org/10.1038/s41598-018-19440-9.
17. Psiuk-Maksymowicz K, Polewczyk A, Orlef A, Walczak E, Czerwiński M, Gąsior Z. Methodology of generation of CFD meshes and 4D shape reconstruction of coronary arteries from patient-specific dynamic CT. Sci Rep. 2024;14:2201-15. https://doi.org/10.1038/s41598-024-52398-5.

File name: Additional file 1.mp4

Title of data: 4D CT Processing Pipeline for Dynamic Coronary Tree Visualization.

Description of data: The complete processing pipeline for a 4D CT dataset is demonstrated in the animation, showing the key steps of segmentation, temporal interpolation, and visualization of the dynamic coronary tree model.

File name: Additional file 2.mp4

Title of data: Coronary Intervention Simulation Using Dynamic Vessel Mesh.

Description of data: This animation demonstrates our dynamic mesh generation method for coronary intervention simulation, showing both mechanical (guide wire-vessel) interactions and fluid dynamics (contrast medium flow). The approach maintains vessel topology and geometry throughout the cardiac cycle, enabling the realistic real-time intervention simulation shown here.

File name: Additional file 3.mp4

Title of data: Coronary Artery Deformation Using Weight Distribution Method.

Description of data: This animation demonstrates our weight distribution method for coronary artery deformation modeling. The approach ensures smooth variation across vessel walls while maintaining local control and non-negative weights—essential for preserving vessel continuity during cardiac motion. The visualization shows the complete deformation validation process, from original mesh through successive deformations using our skinning weight calculation method.

Supplementary Files

This is a list of supplementary files associated with this preprint. Click to download.

- Additionalfile1.mp4
- Additionalfile2.mp4
- Additionalfile3.mp4